

# Multiperiodic magnetic structures in Hubbard superlattices

André L. Malvezzi <sup>(1)</sup>, Thereza Paiva <sup>(2)</sup> and Raimundo R. dos Santos <sup>(2)</sup>

<sup>(1)</sup>Departamento de Física, Faculdade de Ciências, Universidade Estadual Paulista, Cx.P. 473, 17015-970 Bauru SP, Brazil

<sup>(2)</sup>Instituto de Física, Universidade Federal do Rio de Janeiro, Cx.P. 68528, 21945-970 Rio de Janeiro RJ, Brazil

(November 2, 2018)

We consider fermions in one-dimensional superlattices (SL's), modeled by site-dependent Hubbard- $U$  couplings arranged in a repeated pattern of repulsive (i.e.,  $U > 0$ ) and free ( $U = 0$ ) sites. Density Matrix Renormalization Group (DMRG) diagonalization of finite systems is used to calculate the local moment and the magnetic structure factor in the ground state. We have found four regimes for magnetic behavior: uniform local moments forming a spin-density wave (SDW), 'floppy' local moments with short-ranged correlations, local moments on repulsive sites forming long-period SDW's superimposed with short-ranged correlations, and local moments on repulsive sites solely with long-period SDW's; the boundaries between these regimes depend on the range of electronic densities  $\rho$  and on the SL aspect ratio. Above a critical electronic density,  $\rho_{\uparrow\downarrow}$ , the SDW period oscillates both with  $\rho$  and with the spacer thickness. The former oscillation allows one to reproduce all SDW wave vectors within a small range of electronic densities, unlike the homogeneous system. The latter oscillation is related to the exchange oscillation observed in magnetic multilayers. A crossover between regimes of 'thin' to 'thick' layers has also been observed.

## I. INTRODUCTION

Magnetic multilayers have been the subject of intense study over the last decade. The technologically important giant magnetoresistance (GMR) is one of the most interesting aspects of these compounds. Another aspect which has brought attention to multilayers is the oscillation of the exchange coupling between magnetic layers as the spacer layer thickness is varied. While oscillations with single periods have been well understood for some time, *multiperiodicity* has been theoretically predicted,<sup>1,2</sup> and indeed observed, in trilayer materials. Fe/Cr/Fe samples grown by sputtering or molecular-beam epitaxy (MBE) display two periods of oscillation of the exchange coupling: a so-called long-period, of about 10 to 12 monolayers thick, is superimposed to a short-period component of about two monolayers thick.<sup>3</sup> This superposition of short- and long-period components has also been observed in other MBE-fabricated trilayer materials such as Fe/Mn/Fe,<sup>4</sup> Fe/Au/Fe,<sup>5</sup> Fe/Mo/Fe,<sup>6</sup> and Co/Cu/Co.<sup>7</sup> Short-period oscillations, however, disappear if interface quality is not carefully maintained.<sup>3,8,9</sup> Recent experiments<sup>10</sup> in Fe/Cr/Fe show that areas of constant Cr thickness, with diameter larger than 3-4 nm on the interface, are necessary for the development of short-period oscillations. It is therefore believed that multiperiodicity has not yet been observed in multilayers due to interface roughness.

From the theoretical point of view, both the quantum well theory<sup>1</sup> and the so-called RKKY theory<sup>2</sup> can account for many features related to the oscillations of the exchange coupling. For instance, a direct relation between the periods of oscillation and Fermi surface extrema of bulk spacers has been established.<sup>1,2,11</sup> How-

ever, since the notion of a Fermi surface is not widely applicable to strongly correlated systems, a deeper understanding of multiperiodicity is clearly in order, and microscopic models should provide useful insights.

With this in mind, here we investigate the magnetic properties of a one-dimensional superlattice (SL) model<sup>12-14</sup> in which electronic correlations are incorporated and treated nonperturbatively. The model consists of a periodic arrangement of  $L_U$  sites ("layers") in which the on-site coupling is repulsive, followed by  $L_0$  free (i.e.,  $U = 0$ ) sites. The role played by relative layer thicknesses on the magnetic and conducting properties of these systems is then probed by varying  $L_0$  and  $L_U$ .

The SL structure gives rise to several remarkable features,<sup>12</sup> in marked contrast with the otherwise homogeneous system: Local moment maxima can be transferred from repulsive to free sites, and the range of parameters in which this occurs has been expressed in terms of a 'phase diagram'.<sup>13</sup> In addition, spin-density-wave (SDW) quasi-order can be wiped out as a result of frustration, and the SL structure also induces a shift in the density  $\rho_I$  at which a Mott-Hubbard insulating phase sets in.<sup>14</sup> Further, by examining the Luttinger liquid version of the model,<sup>15</sup> one finds that these superlattices provide the means to realize *gapless insulating phases*.<sup>16</sup>

Previous studies of the discrete version of the model<sup>12-14</sup> resorted to Lanczos diagonalization, which sets limits on the system sizes used; for instance, a 24-site lattice size could only be considered for the low- and high-density regimes ( $\rho = 1/6$  and  $\rho = 11/6$ ). Nonetheless, one was still able to probe the period of exchange oscillations for these special densities through the analysis of the magnetic structure factor: the peak position displayed oscillatory behavior with the spacer thickness.<sup>13</sup>

Here we use the Density Matrix Renormalization Group (DMRG) technique<sup>17</sup> to study superlattices longer than the ones available through the Lanczos method. With the aid of the magnetic structure factor, we have been able to probe the periodicity of the superlattice over a wider range of layer thicknesses and densities. As we will see, this has led to significant improvements on the phase diagram previously reported,<sup>13</sup> with the addition of information relative to the regions in which one- and two-period-oscillations are found; as it turned out, these regions are closely related to the behavior of the local moment. We have also been able to observe a crossover between the regimes of thin and thick layers; in the latter regime, the ‘aspect ratio’  $\ell \equiv L_U/L_0$  is the only relevant geometric parameter, whereas the magnetic behavior in the former regime depends on  $L_U$  and  $L_0$  separately.

The layout of the paper is as follows: In Section II we introduce the superlattice model and comment on the calculational procedure. Section III focus on the local moment and how it changes with density and layer thickness. The magnetic structure factor and the periodicity of the superlattices are discussed in Section IV, and Section V summarizes our findings.

## II. MODEL AND CALCULATIONAL PROCEDURE

We define the Hamiltonian as

$$\mathcal{H} = -t \sum_{i, \sigma} \left( c_{i\sigma}^\dagger c_{i+1\sigma} + \text{H.c.} \right) + \sum_i U_i n_{i\uparrow} n_{i\downarrow} \quad (1)$$

where, in standard notation,  $i$  runs over the sites of a one-dimensional lattice,  $c_{i\sigma}^\dagger$  ( $c_{i\sigma}$ ) creates (annihilates) a fermion at site  $i$  in the spin state  $\sigma = \uparrow$  or  $\downarrow$ , and  $n_i = n_{i\uparrow} + n_{i\downarrow}$ , with  $n_{i\sigma} = c_{i\sigma}^\dagger c_{i\sigma}$ ; the on-site Coulomb repulsion is taken to be site-dependent:  $U_i = U > 0$ , for sites within the repulsive layers, and  $U_i = 0$  otherwise.

We consider the Hamiltonian (1) on lattices with  $N_s$  sites and  $N_e$  electrons, and open boundary conditions are used. The appropriate Finite Size Scaling (FSS) parameter, however, is the number of periodic cells,  $N_c = N_s/N_b$ , for a basis with  $N_b = L_U + L_0$  sites. The ground state wave function and energy are obtained by numerical diagonalization using the finite-system density-matrix renormalization group (DMRG) method.<sup>17</sup> We used lattice sizes up to 150 sites, and truncation errors in the DMRG procedure were kept around  $10^{-5}$  or smaller. We have performed a systematic study of the magnetic properties for different values of the Coulomb repulsion  $U$ , different occupation  $\rho = N_e/N_s$  and different configurations  $\{U_i\}$ . Not all configurations  $\{U_i\}$  fit into all sizes and occupations but, since DMRG allows us to study a wide range of lattice sizes, we were able to establish overall trends.

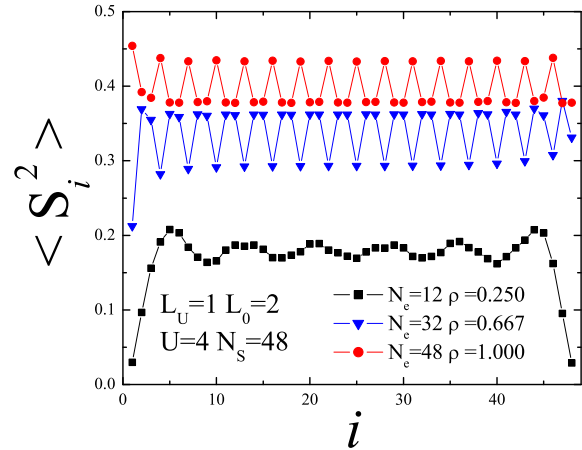


FIG. 1. Local moment as a function of the site ( $i$ ) for the SL with  $L_U = 1$ ,  $L_0 = 2$ ,  $U = 4$ ,  $N_s = 48$ , for  $\rho = 0.25$  (squares),  $\rho = 0.667$  (triangles) and half-filling (circles). The local moment profile changes qualitatively as the density increases.

## III. LOCAL MOMENT PROFILE

The local moment at site  $i$  is defined as  $\langle S_i^2 \rangle = \frac{3}{4} \langle (n_{i\uparrow} - n_{i\downarrow})^2 \rangle$ , and is a measure of both the magnetism and the degree of itinerancy of the system. Figure 1 shows the local moment profile for the SL with  $L_U = 1$ ,  $L_0 = 2$ ,  $U = 4$ ,  $N_s = 48$ , and for three different densities; effects of system size on the local moment are negligible. For small densities, such as for  $\rho = 0.25$ , one identifies small-amplitude oscillations in the local moment profile; their period ( $2\pi/2k_F$ , with  $2k_F = \pi\rho$ ) is determined not by the underlying SL structure, but by the Friedel oscillations in the charge density of the otherwise homogeneous system.<sup>18</sup>

As the density is increased, the SL structure dominates over the Friedel oscillation as evidenced by the data: for  $\rho = 0.667$  the maxima lie on the free sites and the modulation of the profile perfectly matches that of the SL. For large enough densities the maxima migrate to the repulsive sites, as shown by the data for half filling. One should also note that even at the maxima  $\langle S_i^2 \rangle$  is considerably reduced from its value at the completely localized limit ( $U = \infty$ ), namely  $\langle S_i^2 \rangle = 3/4$ ; the itinerant behavior in these cases is therefore evident.

The above example illustrates the existence of three regions, characterized by different local moment profiles: homogeneous (or Friedel-like), free-site peaked, and repulsive-site peaked. In order to locate the boundaries between these regimes it is useful to determine how the local moment at repulsive and free sites separately change with the density. In addition, we define a bias of the local

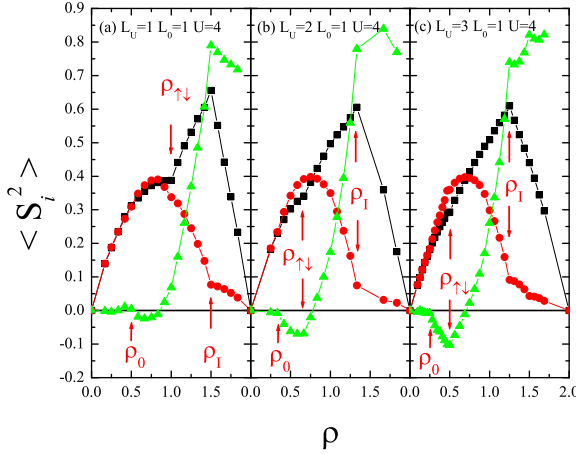


FIG. 2. Bias (triangles) and local moment at repulsive (squares) and free (circles) sites, as functions of density, for  $U = 4$  and for superlattices with (a)  $L_U = L_0 = 1$ ,  $N_s = 24$ ; (b)  $L_U = 2$ ,  $L_0 = 1$ ,  $N_s = 48$ ; and (c)  $L_U = 3$ ,  $L_0 = 1$ ,  $N_s = 64$ .

moment maxima as

$$\delta \equiv \frac{\langle S_U^2 \rangle - \langle S_0^2 \rangle}{\langle S_U^2 \rangle + \langle S_0^2 \rangle}, \quad (2)$$

and also study its dependence with the density.

Figure 2 shows the local moment [both at repulsive ( $\langle S_U^2 \rangle$ ) and free sites ( $\langle S_0^2 \rangle$ )] and the bias as functions of the density, for  $U = 4$ . In the case of Fig. 2,  $L_U \geq L_0$ , with all SL configurations having  $L_0 = 1$ , and  $L_U = 1$  ( $N_s = 24$ ), 2 ( $N_s = 48$ ) and 3 ( $N_s = 64$ ). In order to reduce the effects of open boundary conditions we have averaged over the 6 innermost cells. As the density is increased from the completely empty system, we see that for densities smaller than  $\rho_0$ , given by

$$\rho_0 = \frac{1}{L_0 + L_U}, \quad (3)$$

the local moment increases, and is the same on both sub-lattices (hence  $\delta = 0$ ). For the SL's with  $L_0 = 1$  and  $L_U = 1, 2$  and  $3$  one has  $\rho_0 = 0.5, 0.33$  and  $0.25$ , respectively, which are indicated by arrows in Fig. 2. This density corresponds to having one electron on each cell, so that in the case  $L_U \geq L_0$  electrons have equal probability of being either on a free or on a repulsive site for  $\rho < \rho_0$ .

From Fig. 2 one sees that there is a range of densities above  $\rho_0$ , in which the local moment grows slower on the repulsive sites than on the free ones, since added electrons will preferentially occupy the free sites; hence a negative bias develops within this range. By the same token,  $\langle S_0^2 \rangle$  will reach its maximum value at densities smaller than

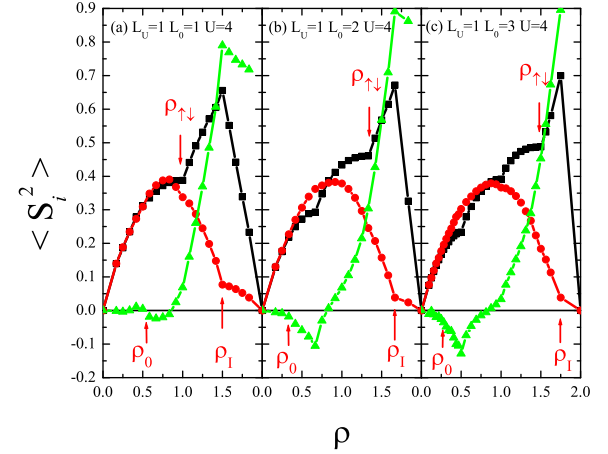


FIG. 3. Bias (triangles) and local moment at repulsive (squares) and free (circles) sites, as functions of density, for  $U = 4$  and for superlattices with (a)  $L_U = L_0 = 1$ ,  $N_s = 24$ ; (b)  $L_U = 1$ ,  $L_0 = 2$ ,  $N_s = 48$ ; and (c)  $L_U = 1$ ,  $L_0 = 3$ ,  $N_s = 64$ .

those at which  $\langle S_U^2 \rangle$  displays its maximum; for completeness, recall that the maximum value of the local moment on a homogeneous free lattice is 0.375, occurring at half filling.

In strong coupling, the free sites saturate at the density

$$\rho_{\uparrow\downarrow} = \frac{2L_0}{L_0 + L_U}, \quad (4)$$

which corresponds to having two electrons on each free site, while the repulsive site is empty. Nonetheless, even for moderate couplings, this density is special. Indeed, from Figs. 2(b) and 2(c) one can see that for  $L_U > L_0$  the bias reaches its minimum value exactly at  $\rho_{\uparrow\downarrow}$ . Also, the local moment at repulsive sites shows a bump at  $\rho_{\uparrow\downarrow}$ , indicating the beginning of a steady occupation of repulsive sites.

Increasing the density even further, one sees that  $\langle S_U^2 \rangle$  reaches its maximum at  $\rho_I$ , defined as

$$\rho_I = \frac{2L_0 + L_U}{L_0 + L_U}, \quad (5)$$

which, in strong coupling, corresponds to having two electrons on each free site and one on each repulsive site; the maximum of  $\langle S_U^2 \rangle$ , at exactly this density, is indicative of the SL being in a Mott-Hubbard insulating state.<sup>14</sup> In the region between  $\rho_{\uparrow\downarrow}$  and  $\rho_I$ , the repulsive layer is preferentially filled as the overall density is increased, causing a steep rise (drop) in the local moment at the repulsive (free) sites. As Fig. 2 shows, the consequence is a steady increase of the bias in this interval.

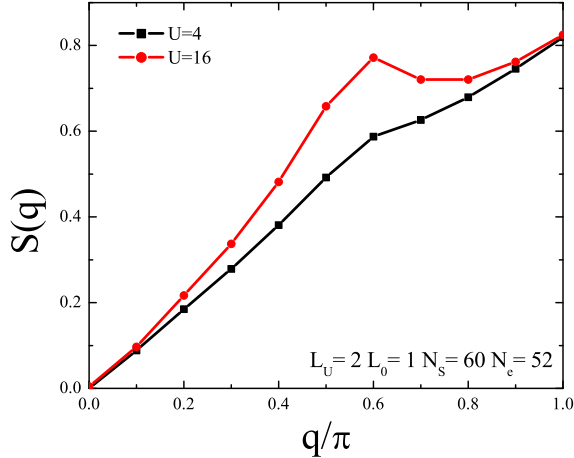


FIG. 4. Magnetic structure factor [Eq. (6)] for a SL with  $L_U = 2$ ,  $L_0 = 1$ ,  $N_s = 60$ ,  $N_e = 52$  (hence  $\rho = 0.87$ ), and for  $U = 4$  and 16.

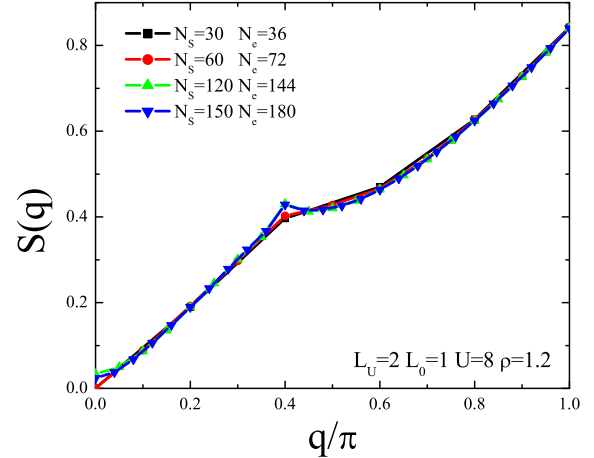


FIG. 5. Magnetic structure factor [Eq. (6)] for a SL with  $L_U = 2$ ,  $L_0 = 1$ ,  $U = 8$ ,  $\rho = 1.2$ , and for different system sizes:  $N_s = 30$  (squares),  $N_s = 60$  (circles),  $N_s = 120$  (up triangles), and  $N_s = 150$  (down triangles).

For densities larger than  $\rho_I$  the free sites are almost completely filled, which is apparent by a considerable decrease in the magnitude of the derivative of  $\langle S_U^2 \rangle$  with respect to the density. Fermions will then start to double occupy the repulsive sites, thus causing a reduction in  $\langle S_U^2 \rangle$ .

The equivalent of Fig. 2 for the case  $L_U \leq L_0$  is shown in Fig. 3. While the overall behavior is the same, a few differences are worth mentioning. The first one is the behavior of the bias in the range  $\rho < \rho_0$ : While the bias vanishes for  $L_U \geq L_0$ , for  $L_U < L_0$  it is negative, though of small magnitude. This is due to the fact that in this range of densities, and within each cell, the electrons have more free sites at their disposal to resonate than repulsive ones; this excess of free sites within each cell also explains why the bias still decreases for densities above  $\rho_0$ .

Second, for  $L_U < L_0$ ,  $\langle S_U^2 \rangle$  is boosted whenever  $\rho = 2m\rho_0$ , with  $m = 1, 2, \dots, L_0 + L_U - 1$ ; this can be attributed to the fact that the double occupancy of the repulsive sites is least likely whenever there are an even number of electrons per cell. Note also that the first bump, at  $2\rho_0$ , coincides with the minimum of the bias.

And, third, while for  $L_U > L_0$  the bias changes sign for  $\rho_{\uparrow\downarrow} < \rho < \rho_I$ , when  $L_U \leq L_0$  this occurs for  $\rho_0 < \rho < \rho_{\uparrow\downarrow}$ ; the actual location of the density at which  $\delta = 0$  depends on the SL configuration, as well as on the Coulomb repulsion  $U$ .

#### IV. MAGNETIC STRUCTURE FACTOR AND EFFECTIVE DENSITIES

Let us now turn to the magnetic structure factor, which is defined as

$$\mathcal{S}(q) = \frac{1}{N_c} \sum_{i,j} e^{iq(r_i - r_j)} \langle \mathbf{S}_i \cdot \mathbf{S}_j \rangle. \quad (6)$$

As  $q$  is related to the repeating units,  $\mathcal{S}(q)$  probes the relative arrangement between different cells. It is important to have in mind that the homogeneous system displays a single peak in the magnetic structure factor at  $q_{max} = 2k_F = \pi\rho$ , for  $\rho \leq 1$ , or  $q_{max} = 2k_F = \pi(2 - \rho)$ , for  $\rho \geq 1$ ,<sup>19</sup> the lattice spacing is taken to be unity throughout this paper.

Figure 4 shows  $\mathcal{S}(q)$  for a SL with  $L_U = 2$ ,  $L_0 = 1$ ,  $\rho = 0.87$ , and for two values of  $U$ , namely  $U = 4$  and  $U = 16$ . Two peaks in the magnetic structure factor are clearly seen in this case: one at  $q = \pi$ , and another at  $q = 3\pi/5$ . While the former is not affected by an increase in  $U$ , the latter grows with  $U$ , though without changing its position. Actually, for sufficiently large  $U$  the peak at  $q \neq \pi$  even becomes more pronounced than the one at  $q = \pi$ . Further data show that this happens for a range of values of  $L_0$ ,  $L_U$ , and  $\rho$ , as discussed below.

The presence of two peaks (at, say,  $q_{max}$  and  $q'_{max}$ , with  $q'_{max} < q_{max}$ ) in the structure factor is associated with a tendency of the system to order (strictly speaking, to *quasi*-order, in one dimension) in a magnetic arrangement dominated by the corresponding periods,  $\lambda = 2\pi/q_{max}$  and  $\lambda' = 2\pi/q'_{max}$ . As we will see

below, the long period oscillates with the spacer thickness, a behavior reminiscent of the exchange oscillation observed in magnetic trilayers.

These two peaks also differ in the way they depend on the system size. Figure 5 shows  $\mathcal{S}(q)$  for the SL with  $L_U = 2$ ,  $L_0 = 1$ ,  $U = 8$ ,  $\rho = 1.2$  ( $\rho_{\uparrow\downarrow} < 1.2 < \rho_I$ ), and for four different lattice sizes, ranging from  $N_s = 30$  to  $N_s = 150$ . From Fig. 5 we see that the inflection already present for  $N_s = 30$  at  $q = 2\pi/5$  sharpens as  $N_s$  increases, and that there is no change in the position of the peak. We have checked that a similar slow, but steady, growth of the peak height with  $N_s$  occurs for the homogeneous Hubbard model away from half filling. These features have been observed for other SL configurations and densities, which therefore indicate that whenever a peak is found at  $q \neq \pi$ , it is robust. On the other hand, the peak at  $q = \pi$  shows a much weaker size-dependence, so that it should be associated with strong, although short-ranged, correlations; this point is illustrated below.

We can then turn to a systematic study of the number of peaks and their positions, by analysing the evolution of the structure factor as the density of electrons is increased. As discussed in Sec. III, for  $\rho < \rho_0$  the local moments are small, and either their maxima are on the free layers, or they are evenly distributed throughout the lattice, depending on whether  $L_U < L_0$  or  $L_U \geq L_0$ , respectively. A small or zero bias signals that the SL structure is not very relevant in this situation. Indeed, the spatial decay of the spin-spin correlation function (not shown here) in the case of a superlattice with a small bias can hardly be distinguished from that of the corresponding homogeneous system; as a result, the magnetic structure factor displays a single peak. In addition, this single peak displays a size- and a  $U$ -dependence similar to those for the homogeneous system.

In order to relate the peak position with some density, one can think of a free (homogeneous) lattice in which the sites are grouped in cells mimicking the SL structure under consideration; it then follows that a meaningful quantity is the *cell density* of electrons,

$$\rho_{\text{cell}} = \frac{N_e}{N_c} = \rho(L_U + L_0), \quad (7)$$

where  $\rho$  is the overall density. For the interacting SL, we have found that the peak position is given by the same expression as for the homogeneous case, but with  $\rho_{\text{cell}}$  replacing  $\rho$ ; that is,

$$q_{\text{max}} = \pi\rho_{\text{cell}}, \quad \text{for } \rho \leq \rho_0. \quad (8)$$

Thus, the peak position grows linearly with  $\rho$  up to  $\rho = \rho_0$  (at which density  $\rho_{\text{cell}} = 1$ ), when it reaches  $q_{\text{max}} = \pi$ ; see Figs. 6 and 7.

The single peak regime persists for  $\rho_0 < \rho < \rho_{\uparrow\downarrow}$ , and, as shown in Figs. 6 and 7, now the peak is always at  $q = \pi$ . The single peaks in this region show a very weak dependence on the system size, which is reflected in the spatial decay of the correlation functions,  $\langle S_0^z S_I^z \rangle$ . As

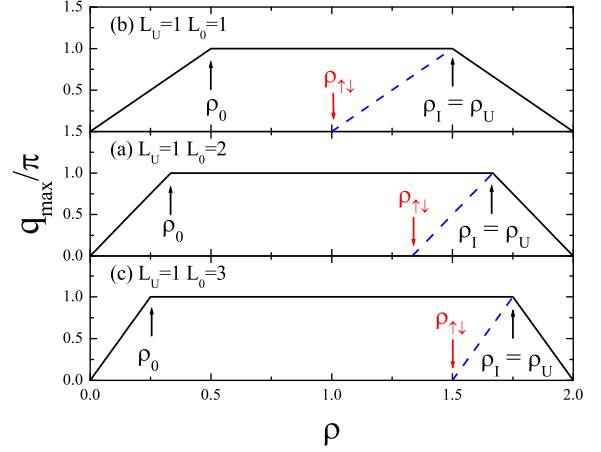


FIG. 6. Maxima position,  $q_{\text{max}}$ , of the magnetic structure factor as a function of density for  $U = 4$ , and (a)  $L_U = 1$   $L_0 = 1$   $N_s = 24$ , (b)  $L_U = 1$   $L_0 = 2$   $N_s = 48$ , and (c)  $L_U = 1$   $L_0 = 3$   $N_s = 64$ . The dashed lines indicate the presence of another peak in  $\mathcal{S}(q)$  (see text).

illustrated in Fig. 8(a) for  $L_U = L_0 = 1$ ,  $U = 4$ , and  $\rho = 0.75$ , correlations with origin in either of the sublattices barely survive at large distances; this should be contrasted with the case displayed in Fig. 8(b), for  $\rho = 1.75$  (see below), in which correlations in one of the superlattices are ‘long’ ranged.

At  $\rho_{\uparrow\downarrow}$ , and in strong coupling, the free layers are completely filled while the repulsive layers are empty. But as the density is increased beyond  $\rho_{\uparrow\downarrow}$ , a second peak emerges, as indicated by the dotted lines in Figs. 6 and 7. This second peak results from the robust moments located on the repulsive sites. Indeed, if one defines an effective electronic density on the *repulsive* layers as

$$\rho_{\text{eff}} = \rho(L_0 + L_U) - 2L_0, \quad (9)$$

where  $\rho$  is the overall density, the long-periods are located at

$$q'_{\text{max}} = \pi\rho_{\text{eff}}. \quad (10)$$

With this definition, it also becomes clear that for  $\rho = \rho_{\uparrow\downarrow}$  there is no net moment at the repulsive layers, since  $\rho_{\text{eff}} = 0$ .

This two peak structure is present until one reaches  $\rho_U$ , defined by

$$\rho_U \equiv 2 - \rho_0, \quad (11)$$

which corresponds to a single hole per cell. One should also have in mind that the overall magnetic arrangement is determined by the long-period (characterized by  $q'_{\text{max}}$ ), since, as discussed above, this is the one increasing with system size.

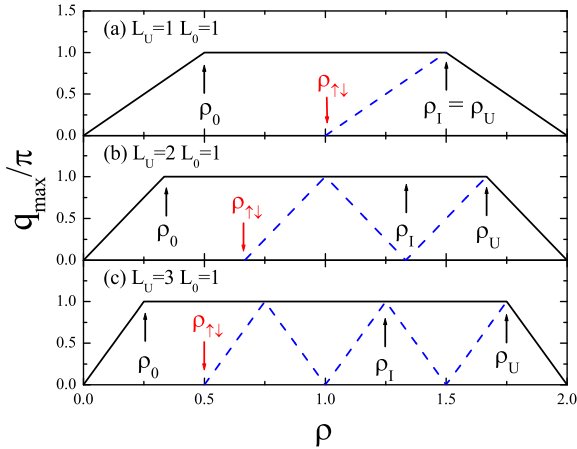


FIG. 7. Maxima position,  $q_{\max}$ , of the magnetic structure factor as a function of density for  $U = 4$ , and  $L_U = 1$   $L_0 = 1$   $N_s = 24$  (a),  $L_U = 2$   $L_0 = 1$   $N_s = 48$  (b), and  $L_U = 3$   $L_0 = 1$   $N_s = 64$  (c). The dashed lines indicate the presence of another peak in  $\mathcal{S}(q)$  (see text).

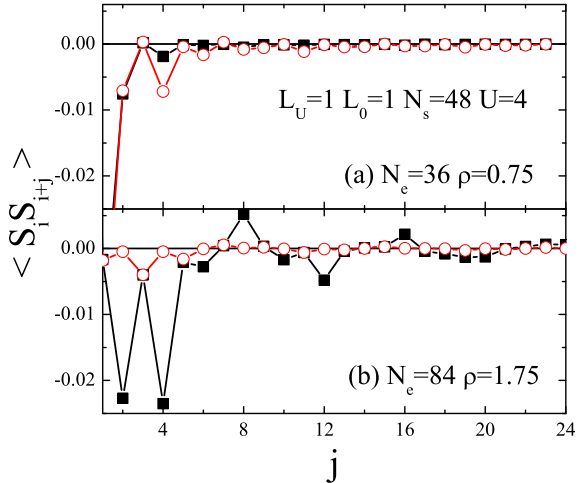


FIG. 8. Spatial decay of correlations, for a SL with  $L_U = L_0 = 1$  and  $U = 4$  for  $N_s = 48$  sites: in (a)  $\rho = 0.75$ , and in (b)  $\rho = 1.75$ . Circles and squares correspond to the origin being taken on free and repulsive sites, respectively.

An interesting difference between the cases depicted in Figs. 6 and 7 is the fact that in the former  $\rho_U = \rho_I$ , while in the latter  $\rho_U > \rho_I$ , and  $q'_{\max}$  is able to go through at least one complete oscillation before  $\rho$  reaches  $\rho_U$ . In this case, the situation  $q'_{\max} = 0$  does not indicate any tendency towards a ferromagnetic arrangement, but is to be associated with *frustration* of the corresponding long-period SDW.<sup>13</sup> Indeed, when  $L_U = 2$  and  $L_0 = 1$  the Mott-Hubbard insulator at  $\rho_I$  is frustrated, since two spins on each repulsive layer form local singlets. Singlets on different repulsive layers, in turn, do not couple with each other, though short ranged correlations are still present; see Fig. 7(b). The frustration at half filling for  $L_U = 3$  and  $L_0 = 1$  can be understood by a similar strong coupling analysis: of the four electrons on each cell, two occupy the free site and the remaining two resonate between three sites, but always forming a singlet. Figure 7(c) shows that further addition of electrons renders these singlets unfavorable, and the system again displays a SDW. At  $\rho = 3/2$ , one reenters a frustrated state, again as a result of having an even number of electrons on the repulsive layer. Therefore, we can relate the reentering frustrated configurations to the formation of singlets on the repulsive layer, which occurs whenever there is an even number of electrons per cell; that is, whenever the density goes through an even multiple of  $2\rho_0$ .

And, finally, above  $\rho_U$  all SL's return to a single peak regime:  $\mathcal{S}(q)$  has a maximum at  $\pi(2 - \rho_{\text{cell}})$  [ $= \pi(2 - \rho_{\text{eff}})$ , since  $\rho_{\text{eff}} = \rho_{\text{cell}} - 2L_0$ ]. The correlations in this regime are quasi-long-ranged, since, as shown in Fig. 8(b), the correlation function with origin at a repulsive site is slowly decaying.

The above analyses of the magnetic structure factor and of the local moment profile can be extended to several other SL configurations, and the outcome can be best summarized by a diagram in the parameter space  $(\rho, L_0, L_U)$ , showing the presence of four different regions (or phases). Cross sections of the full three-dimensional phase diagram are presented in Fig. 9(a) for  $L_U = 1$  and Fig. 9(b) for  $L_U = 4$ . In the low density region (A), located between  $\rho = 0$  and  $\rho = \rho_0$ , the system behaves roughly as if it were homogeneous. The local moments are small and their maxima are located preferentially on the free layers. The SDW is dominated by a single density-dependent wavevector,  $q_{\max} = \pi\rho_{\text{cell}}$ .

At somewhat larger densities,  $\rho_0 < \rho < \rho_{\uparrow\downarrow}$ , lies a region (B), in which the positions of the maxima in the local moment profile depend on the repulsion  $U$ , on  $L_0$ , and  $L_U$ . Presumably as a result of this 'floppy' character of the local moments, spin correlations in this region are strongly antiferromagnetic, but short-ranged.

As the density is further increased, one enters the double-period region ( $C_1$ ), which lies between  $\rho = \rho_{\uparrow\downarrow}$  and  $\rho = \rho_U$ . In this region the local moment on the repulsive layer suffers successive boosts, and one finds SDW's with a 'long' period  $\lambda' = 2/\rho_{\text{eff}}$ ; the latter are accompanied by strong short ranged correlations, of period

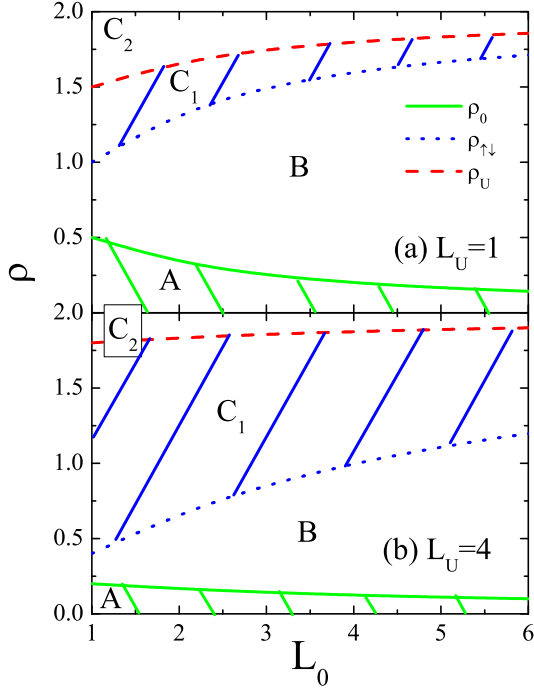


FIG. 9. Regions in the parameter space  $(\rho, L_0)$  for (a)  $L_U = 1$  and (b)  $L_U = 4$ : A – weak moments formed preferentially on free layers and one single SDW period; B – local moment maxima depend on  $U$  and on  $L_0/L_U$  and spin correlations are predominantly antiferromagnetic, but short ranged; C<sub>1</sub> – local moment maxima on the repulsive layers and the SDW's are dominated by two periods; C<sub>2</sub> – local moment maxima on the repulsive layers and the SDW's are dominated by a single period. See text for details. Full line corresponds to  $\rho_0$ , dotted line to  $\rho_{\uparrow\downarrow}$  and dashed line to  $\rho_U$ .

$$\lambda = 2.$$

And, finally, there is a high density region ( $C_2$ ), with densities ranging from  $\rho = \rho_U$  to  $\rho = 2$ . At  $\rho_U$  the local moment bias is maximum (see Figs. 2 and 3), so it decreases as one increases the density. Nonetheless, one still has SDW's, now with a single period given by  $\lambda = 2/(2 - \rho_{\text{cell}})$ . By comparing the two cases depicted in Fig. 9, one sees that a growth of the repulsive layer increases the two-peaked region, at the expense of all others.

The full three-dimensional phase diagram is shown in Fig. 10. The densities  $\rho_0$ ,  $\rho_{\uparrow\downarrow}$ , and  $\rho_U$  define surfaces in the parameter space  $(\rho, L_0, L_U)$  which act as boundaries between the four regions discussed above. The  $\rho_0$ -surface flattens considerably for thick layers, and if one imagines an  $\ell = 1$  line on the horizontal plane of the figure, we see that the homogeneous-like region is only important for moderately thin layers. The  $\rho_{\uparrow\downarrow}$ -surface is the same whether the layers are short or long, since it depends on

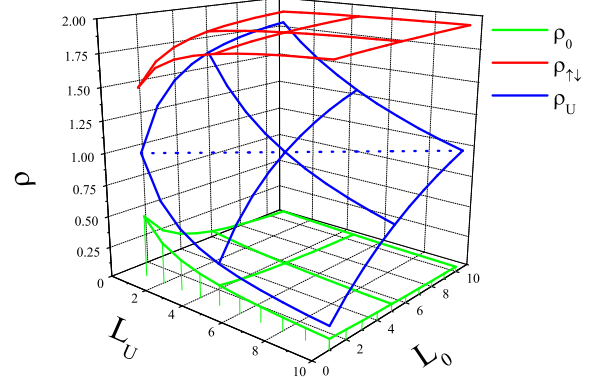


FIG. 10. Regions in the parameter space  $(\rho, L_0, L_U)$ : the lower surface corresponds to  $\rho_0$ , the middle one to  $\rho_{\uparrow\downarrow}$ , and the upper one to  $\rho_U$ . The dotted line is the intersection of the  $\rho_{\uparrow\downarrow}$ -surface with the plane  $\ell = 1$  (see text).

$L_U$  and  $L_0$  only through the combination  $L_U/L_0 \equiv \ell$ ; to illustrate this, the intersection of the  $\rho_{\uparrow\downarrow}$ -surface with the plane  $\ell = 1$ , shown as a dotted line in Fig. 10, yields  $\rho_{\uparrow\downarrow} = 1$  for all  $L_U = L_0$ . The topmost surface ( $\rho_U$ ) also displays a similar crossover between thin and thick regimes: for thick lattices  $\rho_U \rightarrow 2$ .

We are now in a position to discuss the oscillation in  $q_{\text{max}}$  with the spacer (free layer) thickness, for a *fixed electron density*; as mentioned before, these are related to the oscillation of the exchange coupling between magnetic layers. When  $\rho \leq \rho_0$ , one has  $q_{\text{max}} \leq \pi$ , so that there is no oscillatory behavior in  $q_{\text{max}}$ . For  $\rho_0 < \rho \leq \rho_{\uparrow\downarrow}$ , the peak is always at  $q_{\text{max}} = \pi$ , so that again no oscillation is found. Above  $\rho_{\uparrow\downarrow}$ , the long-period maxima in the magnetic structure factor are located at  $q_{\text{max}}(L_0) = \pi\rho_{\text{eff}}(L_0)$ , where we have emphasized the dependence with  $L_0$  through  $\rho_{\text{eff}}$ . We can then calculate the period of oscillation,  $\Delta L_0$ , by setting  $q_{\text{max}}(L_0) = q_{\text{max}}(L_0 + \Delta L_0) \bmod(2\pi)$ . For  $\rho_{\uparrow\downarrow} < \rho \leq 1$  we get

$$\Delta L_0 = \left(1 - \frac{k_F}{\pi}\right)^{-1}, \quad (12)$$

where  $2k_F = \pi\rho$  since  $\rho \leq 1$ ; for  $1 < \rho \leq \rho_U$ , we similarly find

$$\Delta L_0 = \frac{\pi}{k_F}, \quad (13)$$

where now  $2k_F = \pi(2 - \rho)$ . Note that this result is not valid for  $L_U = 1$ , since, according to Fig. 7, once  $q_{\text{max}}$  vanishes, it does not grow as  $L_0$  increases. For  $\rho > \rho_U$ , on the other hand, Eq. (13) is applicable.

We have then established that (i)  $\rho_{\uparrow\downarrow}$  acts as a critical density for the appearance of ‘exchange oscillations’,

and that (ii) our previous results<sup>13</sup> for  $\Delta L_0$ , obtained in the high density region, are valid quite generally for  $\rho > \rho_{\uparrow\downarrow}$ . Further, Eqs. (12) and (13) reproduce previous findings, within the Hartree-Fock approximation, for the periods of oscillation of the exchange coupling in magnetic multilayers.<sup>1,11</sup> Also, the experimentally observed short period of two monolayers reported in Ref. 3 corresponds, in our framework, to the  $\lambda = 2$  correlations. Thus, electronic correlations do not modify the quantum interference effects determining the periods of oscillation from the extrema of the Fermi surface of the spacer material.

## V. CONCLUSIONS

We have investigated one-dimensional Hubbard superlattices consisting of periodic arrangements of free and repulsive layers, by means of Density Matrix Renormalization Group. By considering a much wider range of lattice sizes and densities than in previous studies, we have refined in several aspects our earlier predictions for the magnetic behavior. There are now *four* distinct regimes, depending on the range of electronic densities. For less than one electron per periodic cell, the local moment profile is approximately uniform, and spin-density waves are dominated by a single density-dependent wave vector. When the density lies between those corresponding to one electron per cell and to a fully occupied free sublattice (with empty repulsive sites), maxima in the local moment profile develop, which can be either on free sites or on the repulsive sites, depending on the SL configuration, on the density, and on  $U$ ; also, spin correlations become short ranged, but dominated by a tendency of neighboring cells to align antiparallel. For densities larger than two electrons per free site one has a two-period magnetic structure. There is a long period SDW, in which the wave vector oscillates as a function of the electronic density. An immediate consequence is that SDW's with all possible wave vectors are generated within an interval of densities of  $2\rho_0$ ; this should be compared with the homogeneous system, for which one needs to vary between an empty lattice and a half filled one in order to generate all possible wave vectors. These long-period SDW's are superimposed with short ranged correlations with  $q = \pi$ , which disappear for densities above one hole per periodic cell.

We have also extended to a broader range of densities our earlier prediction that the wave vectors for the SDW's oscillate as the free layer length is varied, with a period determined solely by the electronic density (through the Fermi wave vector). In the context of magnetic multilayers, our results for the period of oscillations exactly reproduce the relation between Fermi surface extrema with exchange coupling oscillation; in addition, the two-monolayer period observed experimentally corresponds in our model to the short period at  $q = \pi$ .

And, finally, we have been able to observe a crossover between the regimes of thin and thick layers; in the latter, the ‘aspect ratio’  $\ell \equiv L_U/L_0$  is the only relevant geometric parameter, whereas in the former regime the magnetic behavior depends on  $L_U$  and  $L_0$  separately. For instance, when any of the layers are thin – less than about 6 sites long –, the SL structure is not felt at low densities, and it behaves as if it were homogeneous; for thick layers, this quasi-homogeneous behavior is only noticeable at very low densities. Similarly, the region of singly peaked correlations at high densities gets smaller as the layers get thicker.

As a final comment, one should expect that the applicability of the one-dimensional model treated here is very close to being extended beyond the realm of higher dimensional superlattices. Indeed, fabrication of nanowire superlattices has been recently reported.<sup>20</sup> Although these superlattices were made up of semiconducting materials, the prospects of growing metallic and/or magnetic *nanosuperlattices* are promising. In this case, our results indicate that a careful control of the doping level leads to a wide variety of distinct magnetic behaviors in the same material. Another possible realization of our model would be to a (as yet hypothetical) superlattice made up of single-walled metallic carbon nanotubes, since these have been successfully described in terms of a Luttinger liquid; see, e.g., Ref. 16 for a partial list of references.

## ACKNOWLEDGMENTS

The authors are grateful to J. d’Albuquerque e Castro, E. Miranda, and J. Silva-Valencia for discussions. Financial support from the Brazilian Agencies CNPq (ALM and RRdS), Fundação de Amparo à Pesquisa do Estado de São Paulo-FAPESP (ALM), FAPERJ (TP and RRdS), and ‘Millenium Institute for Nanosciences/CNPq-MCT’ (RRdS) is also gratefully acknowledged.

---

<sup>1</sup> D. M. Edwards, J. Mathon, R. B. Muniz, and M. S. Phan, Phys. Rev. Lett. **67**, 493 (1991); J. Phys.: Cond. Matter **3**, 4941 (1991).

<sup>2</sup> P. Bruno and C. Chappert, Phys. Rev. Lett. **67**, 1602 (1991); Phys. Rev. B **46**, 261 (1992).

<sup>3</sup> J. Unguris, R. Celotta, and D. Pierce, Phys. Rev. Lett. **67**, 140 (1991).

<sup>4</sup> S. T. Purcell, M. T. Johnson, N. W. E. McGee, R. Coehoorn, and W. Hoving, Phys. Rev. B **45**, 13064 (1992).

<sup>5</sup> A. Fuss, S. Demokritov, P. Grünberg, and W. Zinn, J. Magn. Magn. Mater. **103**, L221 (1992).

<sup>6</sup> Z. Q. Qiu, J. Pearson, A. Berger, and S. D. Bader, Phys. Rev. Lett. **68**, 1398 (1992).

<sup>7</sup> M. T. Johnson, S. T. Purcell, N. W. E. McGee, R. Co-echoorn, J. aan de Stegge, and W. Hoving, Phys. Rev. Lett. **68**, 2688 (1992).

<sup>8</sup> D. Stoeffler and F. Gautier, Phys. Rev. B **44**, 10389 (1991).

<sup>9</sup> J. Wolf, *et al.*, J. Magn. Magn. Mater. **121**, 253 (1993).

<sup>10</sup> C. M. Schmidt, D. E. Bürgler, D. M. Schaller, F. Meisinger, and H.-J. Güntherodt, Phys. Rev. B **60**, 4158 (1999).

<sup>11</sup> J. d'Albuquerque e Castro, M. S. Ferreira, and R. B. Muniz, Phys. Rev. B **49**, 16062 (1994).

<sup>12</sup> T. Paiva and R.R. dos Santos, Phys. Rev. Lett. **76**, 1126 (1996).

<sup>13</sup> T. Paiva and R.R. dos Santos, Phys. Rev. B **62**, 7007 (2000).

<sup>14</sup> T. Paiva and R.R. dos Santos, Phys. Rev. B **58**, 9607 (1998).

<sup>15</sup> J. Silva-Valencia, E. Miranda, and R. R. dos Santos, J. Phys.: Condens. Matter **13**, L619 (2001).

<sup>16</sup> J. Silva-Valencia, E. Miranda, and R. R. dos Santos, Phys. Rev. B **65**, 115115 (2002).

<sup>17</sup> S. R. White, Phys. Rev. Lett. **69**, 2863 (1992); Phys. Rev. B **48**, 10345 (1993).

<sup>18</sup> G. Bedürftig, B. Brendel, H. Frähm, and R. M. Noack, Phys. Rev. B **58**, 10 225 (1998).

<sup>19</sup> H. Frähm and V. Korepin, Phys. Rev. B **42**, 10 553 (1990).

<sup>20</sup> M. S. Gudiksen, L. J. Lauhon, J. Wang, D. C. Smith, and C. M. Lieber, Nature (London) **415**, 617 (2002).